

## Combined Upper Limits on Standard Model Higgs Boson Production from the DØ Experiment in 1.1-3.0 fb<sup>-1</sup>

The DØ Collaboration  
URL <http://www-d0.fnal.gov>  
(Dated: August 2, 2008)

Searches for standard model Higgs boson production in  $p\bar{p}$  collisions at  $\sqrt{s} = 1.96$  TeV have been carried out for Higgs boson masses ( $m_H$ ) in the range  $100 < m_H < 200$  GeV/ $c^2$ . The contributing production processes include associated production ( $WH \rightarrow \ell\nu b\bar{b}$ ,  $ZH \rightarrow \ell\ell/\nu\nu b\bar{b}$ ,  $WH \rightarrow WW^+W^-$ ), gluon fusion ( $H \rightarrow W^+W^-$ ,  $H \rightarrow \gamma\gamma$ ), and vector boson fusion ( $qq'H \rightarrow qq'W^+W^-$ ). Analyses are conducted with integrated luminosities from 1.1 fb<sup>-1</sup> to 3.0 fb<sup>-1</sup>. As no significant excess is observed, we proceed to set limits on standard model Higgs boson production. The observed 95% confidence level upper limits are found to be a factor of 5.3 (2.0) higher than the predicted standard model cross section at  $m_H = 115$  (165) GeV/ $c^2$  while the expected limits are found to be a factor of 4.6 (1.9) higher than the standard model cross section for the same masses.

## I. INTRODUCTION

Despite its success as a predictive tool, the standard model (SM) of particle physics remains incomplete without a means to explain electroweak symmetry breaking. The simplest proposed mechanism involves the introduction of a complex doublet of scalar fields that generate the masses of elementary particles via their mutual interactions. After accounting for longitudinal polarizations for the electroweak bosons, this so-called Higgs mechanism also gives rise to a single scalar boson with an unpredicted mass. Direct searches in  $e^+e^- \rightarrow Z^* \rightarrow ZH$  at the Large Electron Positron (LEP) collider yielded lower mass limits at  $m_H > 114.4 \text{ GeV}/c^2$  [1] while precision electroweak data yield the indirect constraint  $m_H < 160 \text{ GeV}/c^2$  [2], with both limits set at 95% confidence level (C.L.). When also considering the direct limit, the indirect constraint predicts  $m_H < 190 \text{ GeV}/c^2$ , indicating that the range  $110 \leq m_H \leq 200 \text{ GeV}/c^2$  is the most important search region for a SM Higgs boson. The search for a SM Higgs boson is one of the main goals of the Fermilab Tevatron physics program.

In this note, we combine results of direct searches for SM Higgs bosons in  $p\bar{p}$  collisions at  $\sqrt{s} = 1.96 \text{ TeV}$  recorded by the  $D\bar{O}$  experiment [3]. These are searches for Higgs bosons produced in association with vector bosons ( $p\bar{p} \rightarrow WH \rightarrow \ell\nu b\bar{b}$ ,  $p\bar{p} \rightarrow ZH \rightarrow \ell\ell/\nu\nu b\bar{b}$  and  $p\bar{p} \rightarrow WH \rightarrow WW^+W^-$ ), quarks ( $p\bar{p} \rightarrow q\bar{q}H \rightarrow q\bar{q}W^+W^-$ ) or through gluon-gluon fusion ( $p\bar{p} \rightarrow H \rightarrow W^+W^-$ ,  $p\bar{p} \rightarrow H \rightarrow \gamma\gamma$ ). The searches were conducted with data collected during the period 2002-2008 and correspond to integrated luminosities ranging from  $1.1 \text{ fb}^{-1}$  to  $3.0 \text{ fb}^{-1}$ . The searches are organized into twenty final states, each designed to isolate a particular Higgs boson production and decay mode. In order to facilitate proper combination of signals, the analyses were designed to be mutually exclusive after analysis selections. Searches for several final states are performed in two distinct epochs of data collection: before and after the 2006  $D\bar{O}$  detector upgrade. The largest changes made during the upgrade were the addition of a new layer to the silicon detector nearest to the beam-line and an upgrade of the trigger system. The two epochs are denoted as Run IIa ( $1.1\text{fb}^{-1}$ ) and Run IIb (still on-going, currently up to  $1.9\text{fb}^{-1}$  are analyzed in this note). This results in a total of 31 individual analyses.

The 31 analyses used in this combination [4–7, 9–11] are outlined in Table I. In the cases of  $p\bar{p} \rightarrow W/ZH + X$  production, we search for a Higgs boson decaying to two bottom quarks. The decays of the vector bosons further define the analyzed final states:  $WH \rightarrow \ell\nu b\bar{b}$ ,  $ZH \rightarrow \ell\ell b\bar{b}$  and  $ZH \rightarrow \nu\bar{\nu} b\bar{b}$ . To isolate  $H \rightarrow b\bar{b}$  decays, an algorithm for identifying jets consistent with the decay of a heavy-flavor quark is applied to each jet ( $b$ -tagging). Several kinematic variables sensitive to transversely-displaced jet vertices and jet tracks with large transverse impact parameters relative to the hard-scatter vertices are combined in a neural network (NN) discriminant trained to identify real heavy-flavor quark decays and reject jets arising from light-flavor quarks or gluons [14]. By adjusting a minimum requirement on the  $b$ -tagging NN output, a spectrum of increasingly stringent  $b$ -tagging operating points is achieved, each with a different signal efficiency and purity. For the  $WH \rightarrow \ell\nu b\bar{b}$  and  $ZH \rightarrow \ell\ell b\bar{b}$  processes, the analyses are separated into two groups: one in which two of the jets were  $b$ -tagged with a loose tagging requirement (herein called double  $b$ -tag or DT) and one group in which only one jet was tagged with a tight tag algorithm (single  $b$ -tag or ST). The ST selection excludes additional loose-tagged jets, rendering the ST and DT selections orthogonal. The ST selection results in a typical per-jet efficiency and fake rate of about 50% and 0.5%, while the DT selection gives 60% and 1.5%. For these analyses, each lepton flavor of the  $W/Z$  boson decay ( $\ell = e, \mu$ ) is treated as an independent channel. For the  $ZH \rightarrow \nu\bar{\nu} b\bar{b}$  analyses, two or three jets are required in the final state with the two leading jets satisfying a loose  $b$ -tag and one of these jets also satisfying a tight  $b$ -tag. In the case of  $WH \rightarrow \ell\nu b\bar{b}$  production, the primary lepton from the  $W$  boson decay may fall outside of the detector fiducial volume or is not identified. This case is treated as a separate  $WH$  analysis, referred to as  $WH \rightarrow \ell\nu b\bar{b}$ . For this channel, the background is the same as for the  $ZH \rightarrow \nu\bar{\nu} b\bar{b}$  analysis and the  $WH \rightarrow \ell\nu b\bar{b}$  and  $ZH \rightarrow \nu\bar{\nu} b\bar{b}$  searches are combined.

We also consider Higgs decays to two  $W^\pm$  bosons. For  $WH \rightarrow WW^+W^-$  production, we search for leptonic  $W$  boson decays with three final states of same-signed leptons:  $WWW \rightarrow e^\pm\nu e^\pm\nu + X$ ,  $e^\pm\nu\mu^\pm\nu + X$ , and  $\mu^\pm\nu\mu^\pm\nu + X$ . In the case of  $p\bar{p} \rightarrow H \rightarrow W^+W^-$  and  $p\bar{p} \rightarrow q\bar{q}H \rightarrow q\bar{q}W^+W^-$  production via vector boson fusion, we search for leptonic  $W$  boson decays with three final states of opposite-signed leptons:  $WW \rightarrow e^+\nu e^-\nu$ ,  $e^\pm\nu\mu^\mp\nu$ , and  $\mu^+\nu\mu^-\nu$ . For the gluon fusion and vector boson fusion processes,  $H \rightarrow b\bar{b}$  decays are not considered due to the large multijets background. In all  $H \rightarrow W^+W^-$  decays with  $m_H < 2M_W$ , one of the  $W$  bosons will be off mass shell. In all cases, lepton selections include both electrons and muons ( $\ell = e, \mu$ ), but  $\tau$  leptons are included in the simulation and the selections necessarily have acceptance for secondary leptons from  $\tau \rightarrow \nu e, \mu\nu$  decays. Finally, we include an analysis that searches for Higgs bosons decaying to two photons and produced via gluon-gluon fusion, vector boson fusion, and associated production mechanisms. Since the most recent  $D\bar{O}$  SM combined Higgs boson search results [15], we have updated the  $H \rightarrow W^+W^-$  analyses, the Run IIa  $WH \rightarrow \ell\nu b\bar{b}$  analyses, the Run IIb  $ZH \rightarrow \ell\ell b\bar{b}$  analyses, and the  $H \rightarrow \gamma\gamma$  analyses.

Higgs signals are simulated using PYTHIA [16] using CTEQ6M [17] parton distribution functions. The signal cross sections are normalized to next-to-next-to-leading-order (NNLO) calculations [18, 19] and branching ratios are calculated using HDECAY [20]. The  $H \rightarrow W^+W^-$  signal cross sections calculations also contain next-to-

TABLE I: List of analysis channels, corresponding integrated luminosities, and final variables. See Sect. I for details. The final variable used for several analyses is a neural-network or boosted decision-tree discriminant output which is abbreviated as “NN discriminant” and “DTree discriminant”, respectively.

Channel	Data Epoch	Luminosity ( $\text{fb}^{-1}$ )	Final Variable	Reference
$WH \rightarrow e\nu b\bar{b}$ , ST/DT, $W + 2$ jet	Run IIa	1.1	NN discriminant	[4]
$WH \rightarrow e\nu b\bar{b}$ , ST/DT, $W + 3$ jet	Run IIa	1.1	Dijet Mass	[4]
$WH \rightarrow e\nu b\bar{b}$ , ST/DT, $W + 2$ jet	Run IIb	0.6	NN discriminant	[5]
$WH \rightarrow \mu\nu b\bar{b}$ , ST/DT, $W + 2$ jet	Run IIa	1.1	NN discriminant	[4]
$WH \rightarrow \mu\nu b\bar{b}$ , ST/DT, $W + 3$ jet	Run IIa	1.1	Dijet Mass	[4]
$WH \rightarrow \mu\nu b\bar{b}$ , ST/DT, $W + 2$ jet	Run IIb	0.6	NN discriminant	[5]
$WH \rightarrow \ell\nu b\bar{b}$ , DT	Run IIa	0.9	DTree discriminant	[6]
$WH \rightarrow \ell\nu b\bar{b}$ , DT	Run IIb	1.2	DTree discriminant	[6]
$ZH \rightarrow \nu\bar{\nu} b\bar{b}$ , DT	Run IIa	0.9	DTree discriminant	[6]
$ZH \rightarrow \nu\bar{\nu} b\bar{b}$ , DT	Run IIb	1.2	DTree discriminant	[6]
$ZH \rightarrow e^+e^- b\bar{b}$ , ST/DT	Run IIa	1.1	NN discriminant	[7]
$ZH \rightarrow \mu^+\mu^- b\bar{b}$ , ST/DT	Run IIa	1.1	NN discriminant	[7]
$ZH \rightarrow e^+e^- b\bar{b}$ , ST/DT	Run IIb	1.2	NN discriminant	[8]
$ZH \rightarrow \mu^+\mu^- b\bar{b}$ , ST/DT	Run IIb	1.2	DTree discriminant	[8]
$WH \rightarrow WW^+W^- (\mu^\pm\mu^\pm)$	Run IIa	1.1	2-D Likelihood	[9]
$WH \rightarrow WW^+W^- (e^\pm\mu^\pm)$	Run IIa	1.1	2-D Likelihood	[9]
$WH \rightarrow WW^+W^- (e^\pm e^\pm)$	Run IIa	1.1	2-D Likelihood	[9]
$H \rightarrow W^+W^- (\mu^+\mu^-)$	Run IIa+Run IIb	3.0	NN discriminant	[10]
$H \rightarrow W^+W^- (e^\pm\mu^\mp)$	Run IIa+Run IIb	3.0	NN discriminant	[10]
$H \rightarrow W^+W^- (e^+e^-)$	Run IIa+Run IIb	3.0	NN discriminant	[10]
$H \rightarrow \gamma\gamma$	Run IIa+Run IIb	2.7	Di-photon Invariant Mass	[11]

next-to-leading-logarithm corrections [21] and two-loop electroweak corrections [22]. The contributions from QCD multijet production are measured in data. The other backgrounds were generated by PYTHIA, ALPGEN [23], and COMPHEP [24], with PYTHIA providing parton-showering and hadronization. Background cross sections are either normalized to next-to-leading order (NLO) calculations from MCFM [25] or to data control samples whenever possible.

## II. LIMIT CALCULATIONS

We combine results using the  $CL_s$  method with a negative log-likelihood ratio (LLR) test statistic [26]. The value of  $CL_s$  is defined as  $CL_s = CL_{s+b}/CL_b$  where  $CL_{s+b}$  and  $CL_b$  are the confidence levels for the signal-plus-background hypothesis and the background-only hypothesis, respectively. These confidence levels are evaluated by integrating corresponding LLR distributions populated by simulating outcomes via Poisson statistics. Separate channels and bins are combined by summing LLR values over all bins and channels. This method provides a robust means of combining individual channels while maintaining individual channel sensitivities and incorporating systematic uncertainties. Systematics are treated as Gaussian uncertainties on the expected numbers of signal and background events, not the outcomes of the limit calculations. This approach ensures that the uncertainties and their correlations are propagated to the outcome with their proper weights. The  $CL_s$  approach used in this analysis utilizes binned final-variable distributions rather than a single-bin (fully integrated) value for each contributing analysis. The exclusion criteria is determined by increasing the signal cross section until  $CL_s = 1 - \alpha$ , which defines a signal cross section excluded at 95% confidence level for  $\alpha = 0.95$ .

### A. Final Variable Preparation

For the  $WH \rightarrow \ell\nu b\bar{b}$ ,  $ZH \rightarrow \ell\ell b\bar{b}$ , and  $H \rightarrow W^+W^-$  analyses, the final variable used for limit setting is the output of a neural-network (NN) discriminant, trained separately for each Higgs boson mass tested, except for the  $WH \rightarrow \ell\nu b\bar{b}/W + 3$  jet analyses, where the dijet mass is used. For the Run IIa  $H \rightarrow W^+W^-$  analyses, each NN is constructed using kinematic variables which may be different for each Higgs boson mass. The  $WH \rightarrow WW^+W^-$  analysis utilizes a two-dimensional likelihood discriminant as a final variable and the  $ZH \rightarrow \nu\bar{\nu} b\bar{b}$  analyses employ a boosted decision-tree

discriminant. The final variables for all analyses are shown in Figs. 1-4.

Compared to our previous combination, most of the analyses are now performed on a fine Higgs boson mass grid (every 5 GeV). For those still on a 10 GeV grid, additional mass points are created via interpolation of signals and backgrounds [27].

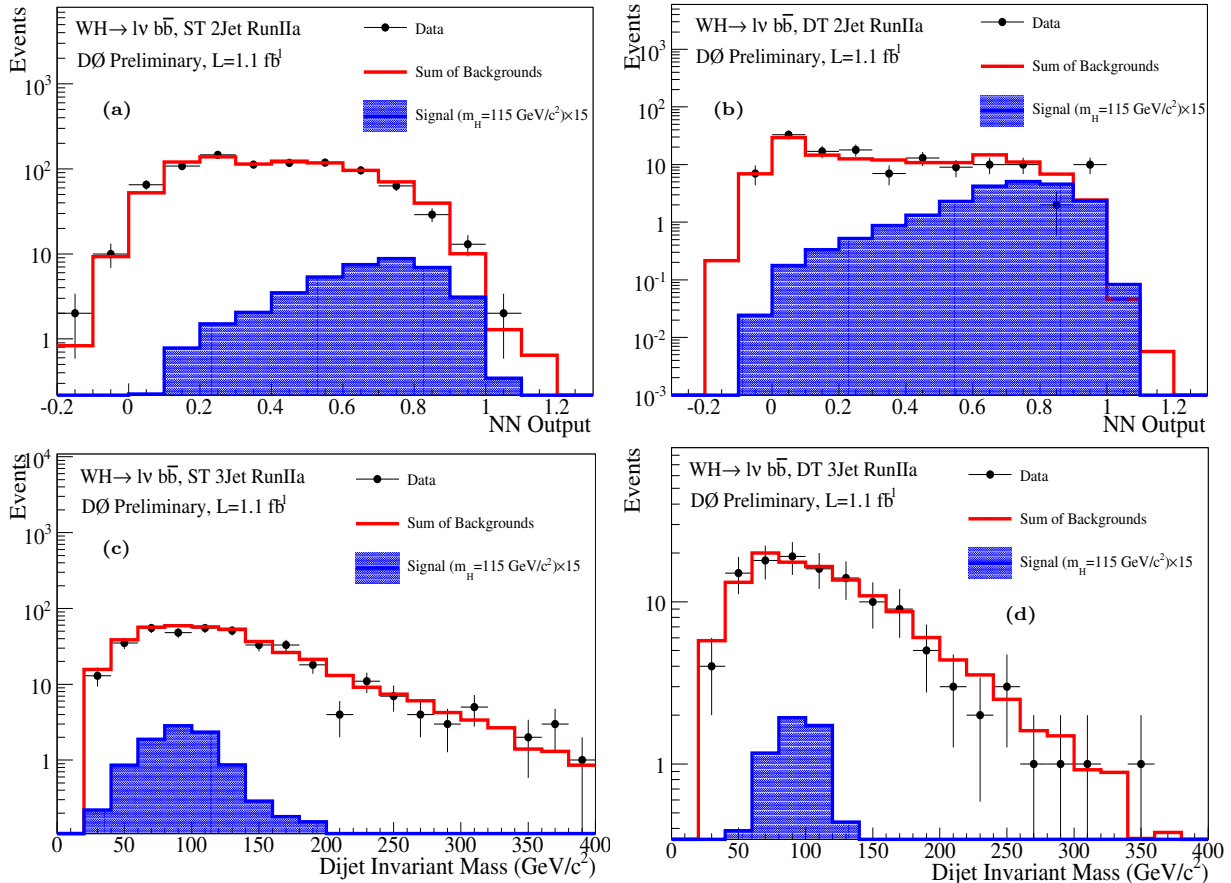


FIG. 1: Final variable distributions for  $p\bar{p} \rightarrow WH \rightarrow l\nu b\bar{b}$  Run IIa Higgs search analyses. The figure contains distributions for: the NN discriminant for the Run IIa  $WH \rightarrow l\nu b\bar{b}$  ST 2-jet analyses (a), the NN discriminant for the Run IIa  $WH \rightarrow l\nu b\bar{b}$  DT 2-jet analyses (b), the dijet invariant mass for the Run IIa  $WH \rightarrow l\nu b\bar{b}$  ST 3-jet analyses (c), and the dijet invariant mass for the Run IIa  $WH \rightarrow l\nu b\bar{b}$  DT 3-jet analyses (d). For each figure, the total signal and background expectations and the observed data are shown.

## B. Systematic Uncertainties

The systematic uncertainties differ between analyses for both the signals and backgrounds [4–7, 9–11]. Here we will summarize only the largest contributions. Most analyses carry an uncertainty on the integrated luminosity of 6.1%, while the overall normalization of other analyses is determined from the NNLO  $Z/\gamma^*$  cross section in data events near the peak of  $Z \rightarrow \ell\ell$  decays in data. The  $H \rightarrow b\bar{b}$  analyses have an uncertainty on the  $b$ -tagging rate of 2-6% per tagged jet. These analyses also have an uncertainty on the jet measurement and acceptances of  $\sim 7.5\%$ . For the  $H \rightarrow W^+W^-$  analyses we include uncertainties associated with lepton measurement and acceptances, which range from 3-6% depending on the final state. The largest contribution for all analyses is the uncertainty on the background cross sections at 6-30% depending on the analysis channel and specific background. These values include both the uncertainty on the theoretical cross section calculations and the uncertainties on the higher order correction factors. The uncertainty on the expected multijet background is dominated by the statistics of the data sample from which it is estimated, and is considered separately from the other cross section uncertainties. The  $p\bar{p} \rightarrow H \rightarrow W^+W^-$  and  $H \rightarrow \gamma\gamma$  analyses are also assigned a 10% uncertainty on the NNLO Higgs production cross section associated with the accuracy of the theoretical calculation. In addition, several analyses incorporate shape-dependent uncertainties on the

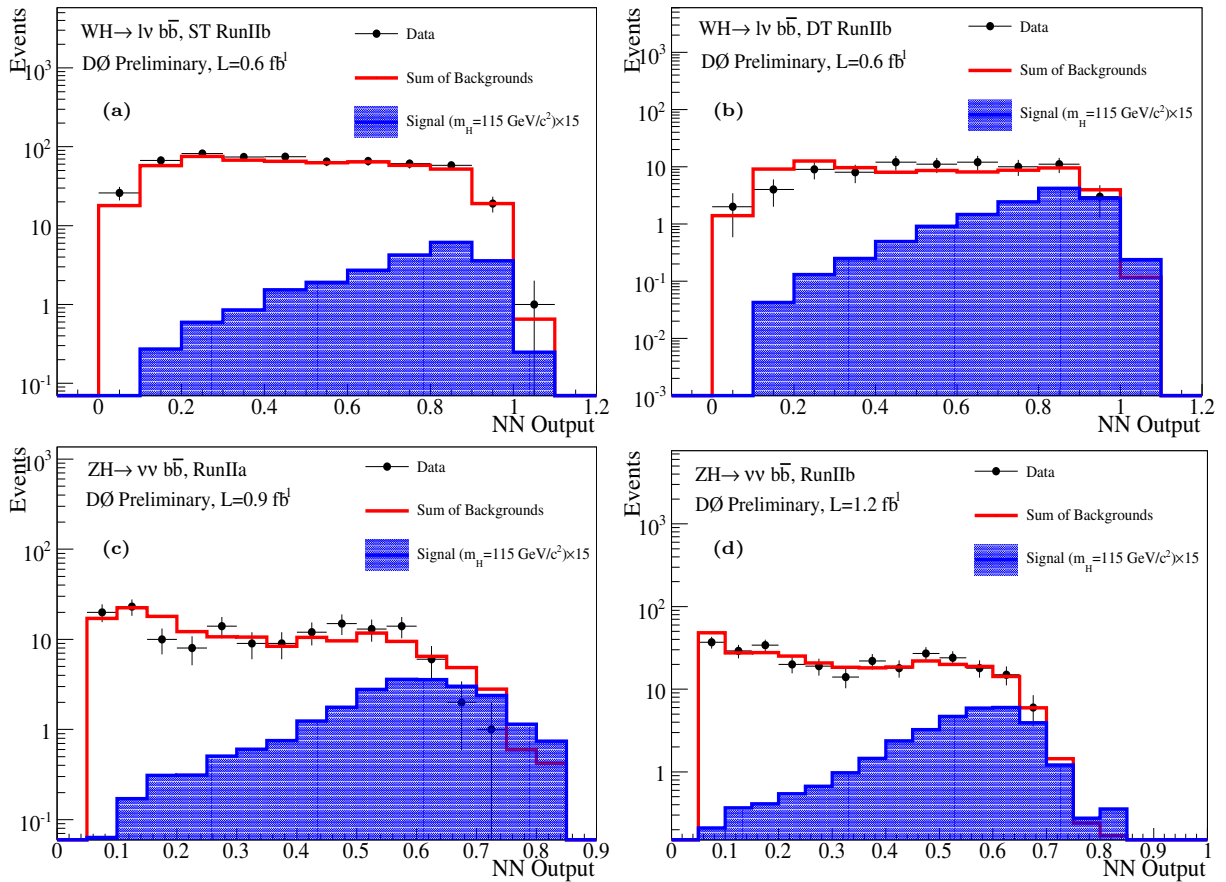


FIG. 2: Final variable distributions for the Run IIB  $p\bar{p} \rightarrow WH \rightarrow \ell\nu b\bar{b}$  and the  $p\bar{p} \rightarrow ZH \rightarrow \ell\ell/\nu\nu b\bar{b}$  Higgs search analyses. The figure contains distributions for: the NN discriminant for the Run IIB  $WH \rightarrow \ell\nu b\bar{b}$  ST analyses (a), the NN discriminant for the Run IIB  $WH \rightarrow \ell\nu b\bar{b}$  DT analyses (b), the DTree discriminant for the Run IIA  $ZH \rightarrow \nu\bar{\nu} b\bar{b}$  analysis (c), and the DTree discriminant for the Run IIB  $ZH \rightarrow \nu\bar{\nu} b\bar{b}$  analysis (d). For each figure, the total signal and background expectations and the observed data are shown.

kinematics of the dominant backgrounds in the analyses. These shapes are derived from the potential deformations of the final variables due to generator and background modeling uncertainty. Further details on the systematic uncertainties are given in Table II.

The systematic uncertainties for background rates are generally several times larger than the signal expectation itself and are an important factor in the calculation of limits. As such, each systematic uncertainty is folded into the signal and background expectations in the limit calculation via Gaussian distribution. These Gaussian values are sampled for each Poisson MC trial (pseudo-experiment). Several of the systematic uncertainties, for example the jet energy scale uncertainty, impact the shape of the final variable. These shape-dependencies were preserved in the description of systematic fluctuations for each Poisson trial. Correlations between systematic sources are carried through in the calculation. For example, the uncertainty on the integrated luminosity is held to be correlated between all signals and backgrounds and, thus, the same fluctuation in the luminosity is common to all channels for a single pseudo-experiment. All systematic uncertainties originating from a common source are held to be correlated, as detailed in Tables II and III.

To minimize the degrading effects of systematics on the search sensitivity, the individual background contributions are fitted to the data observation by maximizing a profile likelihood function for each hypothesis [28]. The profile likelihood is constructed via a joint Poisson probability over the number of bins in the calculation and is a function of the nuisance parameters in the system and their associated uncertainties, which are given an additional Gaussian constraint associated with their prior predictions. The maximization of the likelihood function is performed over the nuisance parameters. A fit is performed to both the background-only and signal-plus-background hypotheses separately for each Poisson MC trial.

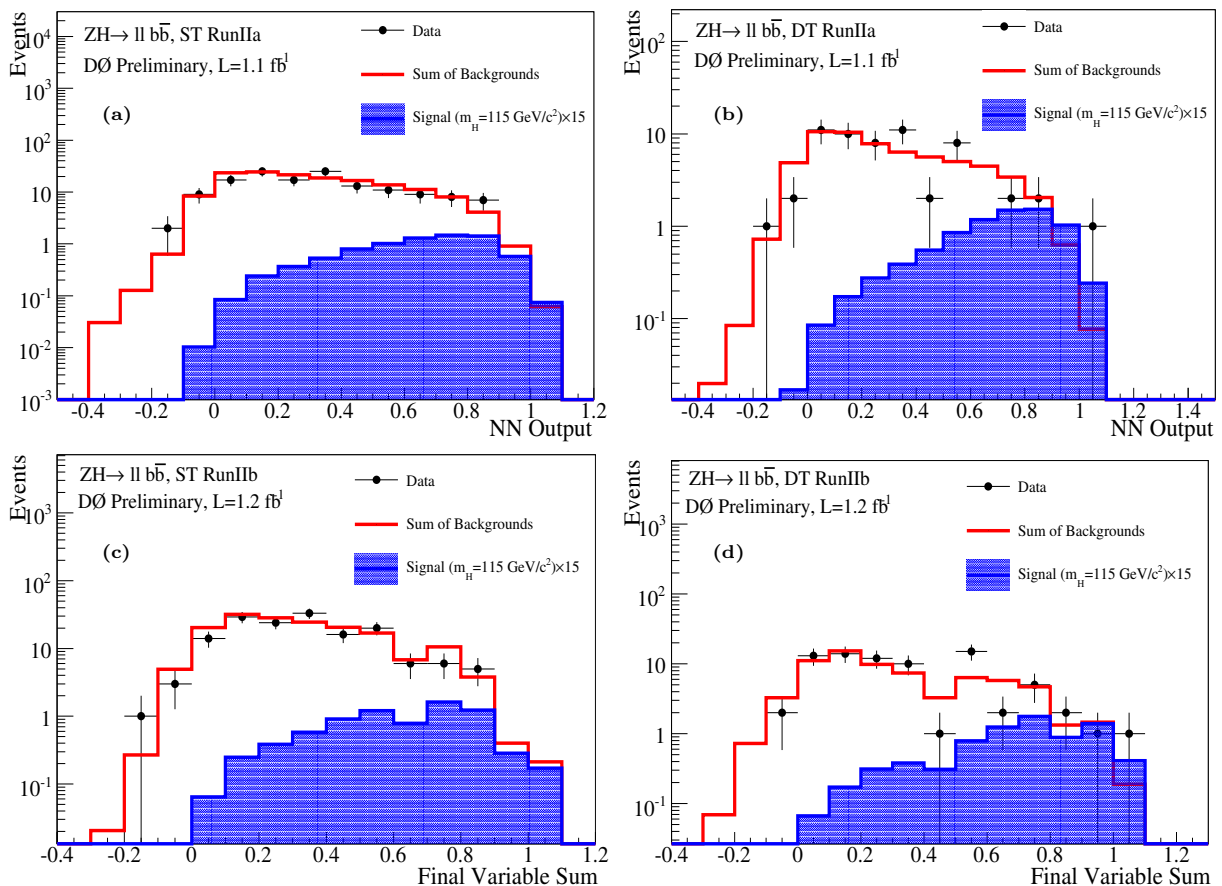


FIG. 3: Final variable distributions for the  $ZH \rightarrow \ell\ell b\bar{b}$  Higgs search analyses. The figure contains distributions for: the NN discriminant for the Run Ila ST  $ZH \rightarrow \ell\ell b\bar{b}$  analyses (a), the NN discriminant for the Run Ila DT  $ZH \rightarrow \ell\ell b\bar{b}$  analyses (b), the NN discriminant for the Run Iib ST  $ZH \rightarrow \ell\ell b\bar{b}$  analyses (c), and the NN discriminant for the Run Iib DT  $ZH \rightarrow \ell\ell b\bar{b}$  analyses (d). For each figure, the total signal and background expectations and the observed data are shown.

### III. DERIVED UPPER LIMITS

We derive limits on SM Higgs boson production  $\sigma \times BR(H \rightarrow b\bar{b}/W^+W^-)$  via 31 individual analyses [4–7, 9–11]. The limits are derived at a 95% C.L. To facilitate model transparency and to accommodate analyses with different degrees of sensitivity, we present our results in terms of the ratio of 95% C.L. upper cross section limits to the SM predicted cross section as a function of Higgs boson mass. The SM prediction for Higgs boson production would therefore be considered excluded at 95% C.L. when this limit ratio falls below unity. For the combined limit, the  $WH \rightarrow \ell\nu b\bar{b}$  and  $ZH \rightarrow \nu\bar{\nu} b\bar{b}$  signals are summed and their common background only enters the calculation once.

The individual analyses described above are grouped to evaluate combined limits over the range  $100 \leq m_H \leq 200 \text{ GeV}/c^2$ . The  $WH \rightarrow \ell\nu b\bar{b}$  and  $ZH \rightarrow \nu\bar{\nu} b\bar{b}$  analyses contribute to the region  $m_H \leq 145 \text{ GeV}/c^2$ , the  $ZH \rightarrow \ell\ell b\bar{b}$  analyses contribute for  $m_H \leq 150 \text{ GeV}/c^2$ , the Run Ila  $WH \rightarrow WW^+W^-$  analyses contribute for  $m_H \geq 120 \text{ GeV}/c^2$ , the  $H \rightarrow W^+W^-$  analyses contribute for  $m_H \geq 115 \text{ GeV}/c^2$ , and the  $H \rightarrow \gamma\gamma$  analyses contribute for  $m_H \leq 150 \text{ GeV}/c^2$ .

Figure 5 shows the expected and observed 95% C.L. cross section limit ratio to the SM cross sections for all analyses combined over the probed mass region ( $100 \leq m_H \leq 200 \text{ GeV}/c^2$ ). The LLR distributions for the full combination are shown in Fig. 6. Included in these figures are the median LLR values for the signal-plus-background hypothesis ( $LLR_{s+b}$ ), background-only hypothesis ( $LLR_b$ ), and the observed data ( $LLR_{obs}$ ). The shaded bands represent the 1 and 2 standard deviation ( $\sigma$ ) departures for  $LLR_b$ . These distributions can be interpreted as follows:

- The separation between  $LLR_b$  and  $LLR_{s+b}$  provides a measure of the discriminating power of the search. This is the ability of the analysis to separate the  $s+b$  and  $b$ -only hypotheses.

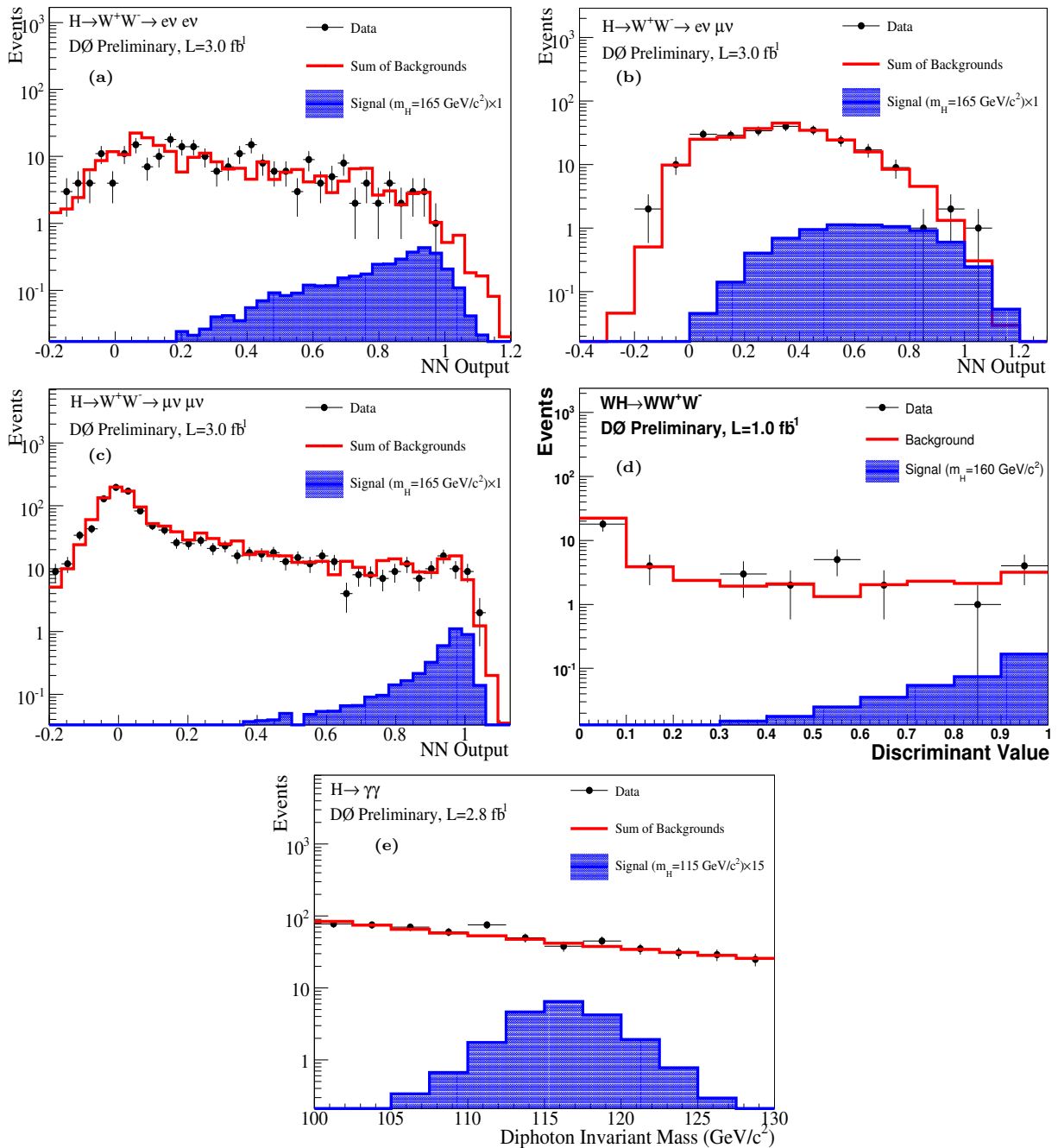


FIG. 4: Final variable distributions for selected Higgs search analyses. The figure contains distributions for: the NN discriminant for the  $H \rightarrow W^+W^- \rightarrow e\nu, e\nu$  analysis (a), the NN discriminant for the  $H \rightarrow W^+W^- \rightarrow e\nu, \mu\nu$  analysis (b), the NN discriminant for the  $H \rightarrow W^+W^- \rightarrow \mu\nu, \mu\nu$  analysis (c), a one-dimensional projection of the two-dimensional likelihood for the Run II  $WH \rightarrow WW^+W^-$  analyses (d), and the diphoton invariant mass for the  $H \rightarrow \gamma\gamma$  analysis (e). For each figure, the total signal and background expectations and the observed data are shown.

- The width of the  $\text{LLR}_b$  distribution (shown here as one and two standard deviation ( $\sigma$ ) bands) provides an estimate of how sensitive the analysis is to a signal-like background fluctuation in the data, taking account of the presence of systematic uncertainties. For example, when a  $1\sigma$  background fluctuation is large compared to the signal expectation, the analysis sensitivity is thereby limited.
- The value of  $\text{LLR}_{obs}$  relative to  $\text{LLR}_{s+b}$  and  $\text{LLR}_b$  indicates whether the data distribution appears to be more like signal-plus-background or background-only. As noted above, the significance of any departures of  $\text{LLR}_{obs}$

TABLE II: List of leading correlated systematic uncertainties. The values for the systematic uncertainties are the same for the  $ZH \rightarrow \nu\bar{\nu}b\bar{b}$  and  $WH \rightarrow \ell\nu b\bar{b}$  channels. All uncertainties within a group are considered 100% correlated across channels. The correlated systematic uncertainty on the background cross section ( $\sigma$ ) is itself subdivided according to the different background processes in each analysis.

Source	$WH \rightarrow e\nu b\bar{b}$ DT(ST)	$WH \rightarrow \mu\nu b\bar{b}$ DT(ST)	$WH \rightarrow WW^+W^-$	$H \rightarrow W^+W^-$
Luminosity (%)	6.1	6.1	-	-
Normalization (%)	-	-	6.1	4-6
Jet Energy Scale (%)	3.0	3.0	0	3.0
Jet ID (%)	3.0	3.0	-	-
Electron ID/Trigger (%)	6.0	-	11	3-10
Muon ID/Trigger (%)	-	7.0	11	7.7-10
$b$ -Jet Tagging (%)	6(3)	6(3)	-	-
Background $\sigma$ (%)	6-20	6-20	6-18	6-18
Signal $\sigma$ (%)	0	0	0	10.0
QCD multijets (%)	14	14	30-50	15-40
Shape-Dependent Bkgd Modeling (%)	5-10	5-10	-	5-20

Source	$ZH \rightarrow \nu\bar{\nu}b\bar{b}$	$ZH \rightarrow e^+e^-b\bar{b}$ DT(ST)	$ZH \rightarrow \mu^+\mu^-b\bar{b}$ DT(ST)	$H \rightarrow \gamma\gamma$
Luminosity (%)	6.1	6.1	-	6.1
Normalization (%)	-	-	6.1	-
Jet Energy Scale (%)	3.0	2.0	2.0	-
Jet ID (%)	2.0	5.0	5.0	-
Jet Triggers (%)	5.5	-	-	-
Electron ID/Trigger (%)	0	4.0	-	12-17
Muon ID/Trigger (%)	0	-	4.0	-
$b$ -Jet Tagging (%)	6.0	7.5(3.0)	7.5(3.0)	-
Background $\sigma$ (%)	6-16	10-30	10-30	5-26
Heavy-Flavor Scale (%)	50	-	-	-
QCD multijets (%)	-	41-50	50	20
Shape-Dependent Bkgd Modeling (%)	-	5-10	5-10	1-5

TABLE III: The correlation matrix for the analysis channels. The correlations for the  $ZH \rightarrow \nu\bar{\nu}b\bar{b}$  and  $WH \rightarrow \ell\nu b\bar{b}$  channels are held to be the same. All uncertainties within a group are considered 100% correlated across channels. The correlated systematic uncertainty on the background cross section ( $\sigma$ ) is itself subdivided according to the different background processes in each analysis.

Source	$WH \rightarrow \ell\nu b\bar{b}$	$ZH \rightarrow \nu\bar{\nu}b\bar{b}$	$ZH \rightarrow \ell\ell b\bar{b}$	$H \rightarrow W^+W^-$	$WH \rightarrow WW^+W^-$	$H \rightarrow \gamma\gamma$
Luminosity	×	×	×			×
Normalization			×	×	×	
Jet Energy Scale	×	×	×	×		
Jet ID	×	×	×			
Electron ID/Trigger	×	×	×	×	×	×
Muon ID/Trigger	×		×	×	×	
$b$ -Jet Tagging	×	×	×			
Background $\sigma$	×	×	×	×	×	×
Background Modeling						
Signal $\sigma$				×		
QCD multijets (%)						

from  $LLR_b$  can be evaluated by the width of the  $LLR_b$  distribution.

The behavior of  $LLR_{obs}$  in Figure 6 and the observed limit in Figure 5 in the range of  $160 \leq m_H \leq 175$  has been studied carefully for any biases in analytical technique. The two  $0.5 - \sigma$  steps taken moving from  $160 \leq m_H \leq 170$  are driven by the statistical variations in the neural-network training cycles and the training samples of the  $H \rightarrow W^+W^-$  analyses. Studies of the behavior of neural-networks trained for neighboring mass points indicate residual fluctuations on the scale of  $0.25 - 0.5 - \sigma$  for the observed data.

TABLE IV: Combined 95% C.L. limits on  $\sigma \times BR(H \rightarrow b\bar{b}/W^+W^-)$  for SM Higgs boson production. The limits are reported in units of the SM production cross section times branching fraction.

$m_H$ ( GeV/ $c^2$ )	100	105	110	115	120	125	130	135	140	145	150
Expected:	3.6	3.9	4.3	4.6	5.0	5.5	5.1	5.0	4.5	4.1	3.2
Observed:	3.9	4.2	4.8	5.3	6.8	7.3	8.7	9.5	7.4	6.4	3.9
$m_H$ ( GeV/ $c^2$ )	155	160	165	170	175	180	185	190	195	200	
Expected	2.8	2.1	1.9	2.3	2.8	3.2	4.6	5.5	6.7	7.4	
Observed	3.2	3.0	2.0	1.7	2.3	2.5	3.6	5.6	5.4	5.6	

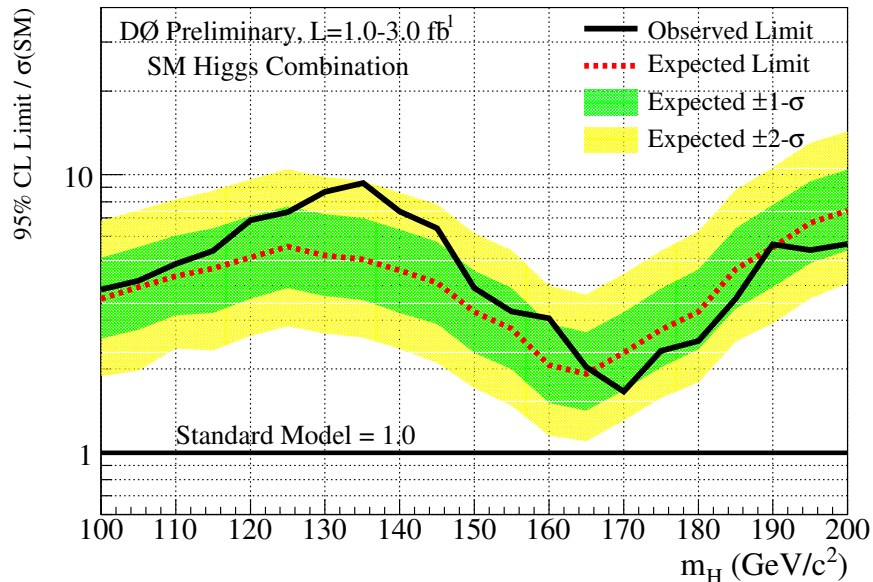


FIG. 5: Expected (median) and observed 95% C.L. cross section upper limit ratios for the combined  $WH/ZH/H, H \rightarrow b\bar{b}/W^+W^-/\gamma\gamma$  analyses over the  $100 \leq m_H \leq 200$  GeV/ $c^2$  mass range.

#### IV. CONCLUSIONS

We have presented upper limits on standard model Higgs boson production derived from 31 Higgs search analyses. We have combined these analyses and form new limits more sensitive than each individual limit. The observed (expected) 95% C.L. upper limit ratios to the SM Higgs boson production cross sections are 5.3 (4.6) at  $m_H = 115$  GeV/ $c^2$  and 2.0 (1.9) at  $m_H = 165$  GeV/ $c^2$ .

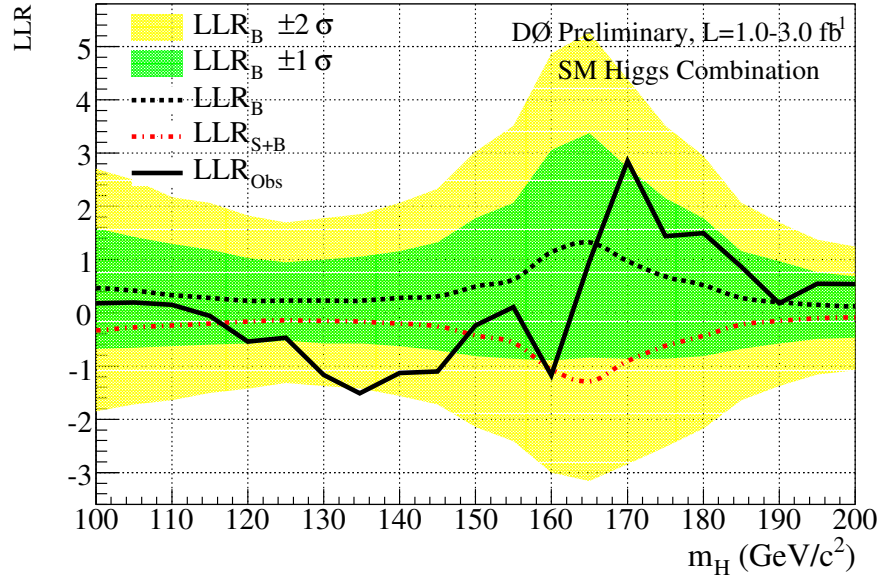


FIG. 6: Log-likelihood ratio distribution for the combined  $WH/ZH/H, H \rightarrow b\bar{b}/W^+W^-/\gamma\gamma$  analyses over the  $100 \leq m_H \leq 200$   $\text{GeV}/c^2$  mass range.

#### Acknowledgments

We thank the staffs at Fermilab and collaborating institutions, and acknowledge support from the DOE and NSF (USA), CEA and CNRS/IN2P3 (France), FASI, Rosatom and RFBR (Russia), CNPq, FAPERJ, FAPESP and FUNDUNESP (Brazil), DAE and DST (India), Colciencias (Colombia), CONACyT (Mexico), KRF and KOSEF (Korea), CONICET and UBACyT (Argentina), FOM (The Netherlands), STFC (United Kingdom), MSMT and GACR (Czech Republic), CRC Program, CFI, NSERC and WestGrid Project (Canada), BMBF and DFG (Germany), SFI (Ireland), The Swedish Research Council (Sweden), CAS and CNSF (China), and the Alexander von Humboldt Foundation.

- 
- [1] R. Barate *et al.* [LEP Working Group for Higgs boson searches], Phys. Lett. B **565**, 61 (2003), [arXiv:hep-ex/0306033].  
[2] LEP Electroweak Working Group: <http://lepewwg.web.cern.ch/LEPEWWG/plots/winter2007/>.  
[3] DØ Collaboration, V. Abazov *et al.*, Nucl. Instrum. Meth. A **565**, 463 (2006) [arXiv:hep-ph/0507191].  
[4] DØ Collaboration, “A Search for Associated  $W$  and Higgs Production in  $p\bar{p}$  Collisions at  $\sqrt{s} = 1.96$  TeV”, to be submitted to Phys. Rev. Lett.  
[5] DØ Collaboration, DØ Note 5472-CONF.  
[6] DØ Collaboration, DØ Note 5586-CONF.  
[7] DØ Collaboration, DØ Note 5482-CONF.  
[8] DØ Collaboration, DØ Note 5570-CONF.  
[9] DØ Collaboration, DØ Note 5485-CONF.  
[10] DØ Collaboration, DØ Note 5757-CONF.  
[11] DØ Collaboration, DØ Note 5737-CONF.  
[12] DØ Collaboration, DØ Note 5669-CONF.  
[13] DØ Collaboration, DØ Note 5739-CONF.  
[14] T. Scanlon, FERMILAB-THESIS-2006-43.  
[15] DØ Collaboration, DØ Note 5625-CONF.  
[16] T. Sjöstrand, P. Edén, C. Friberg, L. Lönnblad, G. Miu, S. Mrenna and E. Norrbin, Computer Phys. Commun. **135** 238 (2001) [arXiv:hep-ph/0010017].  
[17] J. Pumplin *et al.*, JHEP **0207**, 012 (2002).  
[18] S. Catani *et al.*, JHEP **0307**, 028 (2003) [arXiv:hep-ph/0306211].  
[19] K. A. Assamagan *et al.* [Higgs Working Group Collaboration], arXiv:hep-ph/0406152.  
[20] A. Djouadi, J. Kalinowski and M. Spira, Comput. Phys. Commun. **108**, 56 (1998) [arXiv:hep-ph/9704448].  
[21] G. Bozzi, S. Catani, D. de Florian and M. Grazzini, Nucl. Phys. B **971**, 1 (2008)

- [22] U. Aglietti, R. Bonciani, G. Degrossi and A. Vicini, [arXiv:hep-ph/0610033].
- [23] M. L. Mangano *et al.*, JHEP **0307**, 001 (2003) [arXiv:hep-ph/0206293].
- [24] A. Pukhov *et al.*, arXiv:hep-ph/9908288.
- [25] <http://mcfm.fnal.gov/>.
- [26] T. Junk, Nucl. Instrum. Meth. A **434**, 435 (1999); A.Read, CERN 2000-005 (30 May 2000).
- [27] A. Read, Nucl. Instrum. Meth. A **425**, 357 (1999).
- [28] W. Fisher, FERMILAB-TM-2386-E.